Hindawi Publishing Corporation
Shock and Vibration
Volume 2014, Article ID 524351, 10 pages
http://dx.doi.org/10.1155/2014/524351

Research Article

Experimental Research on an Active Sting Damper in a Low Speed Acoustic Wind Tunnel

Jinjin Chen, Xing Shen, Fanfan Tu, and Ehtesham Mustafa Qureshi

State Key Laboratory of Mechanics and Control of Mechanical Structures, Nanjing University of Aeronautics and Astronautics, Nanjing 210016, China

Correspondence should be addressed to Xing Shen; shenx@nuaa.edu.cn

Received 27 September 2013; Revised 17 February 2014; Accepted 17 February 2014; Published 6 March 2014

Academic Editor: Mohammad Elahinia

Wind tunnels usually use long cantilever stings to support aerodynamic models in order to reduce support system flow interference on experimental data. However, such support systems are a potential source of vibration problems which limit the test envelope and affect data quality due to the inherently low structural damping of the systems. When exposed to tunnel flow, turbulence and model flow separation excite resonant Eigenmodes of a sting structure causing large vibrations due to low damping. This paper details the development and experimental evaluation of an active damping system using piezoelectric devices with balance signal feedback both in a lab and a low speed acoustic wind tunnel and presents the control algorithm verification tests with a simple cantilever beam. It is shown that the active damper, controlled separately by both PID and BP neural network, has effectively attenuated the vibration. For sting mode only, 95% reduction of displacement response under exciter stimulation and 98% energy elimination of sting mode frequency have been achieved.

1. Introduction

In wind tunnels, aerodynamic models are usually mounted on long cantilever stings to avoid support interference on experimental data during wind tunnel tests. The use of such long cantilever stings can lead to model vibrations relative to flow streamlines and sometimes result in wind tunnel balance overloads [1]. A cantilever sting system consists of a model, a wind tunnel balance, and a tapered hollow sting mounted on a rigid model attitude support system which is a multidegree of freedom spring-mass elastic system. The sting system is exposed to aerodynamic loads from flow dynamic pressure. The amplitude of dynamic response of the sting is a function of damping. Most of the wind tunnel sting systems show six dominant Eigenmodes. These modes are the sting modes in pitch and yaw, coupled-yaw sting modes manifesting as roll mode, model-balance modes in pitch and yaw, and an axial translational model-balance mode [2]. The damping in sting systems exposed to flow comprised aerodynamic damping of the test and sting structural damping. Due to poor structural damping in cantilevers, the spring-mass sting system tends to respond dynamically at these Eigenmodes, when the system is exposed to forces from wide band flow turbulence, model flow separation induced disturbances, and support system dynamics [3].

Many methods have already been tried to improve the sting damping. In 1968, NASA Langley Research Center engineers Igoe and Capone [4] used tuned passive dampers inside a wind tunnel model to suppress the sting mode but only achieved limited success. A second concept that has been used to improve damping in stings is the application of friction springs at NLR by Fuykschot [5]. A third concept is the use of gyroscopic stability to improve damping. Active damping has become feasible with the advent of high force piezoelectric devices. The European Transonic Wind Tunnel (ETW) developed an early design of an active sting damper by using piezoelectric actuators and accelerometer feedback [6]. ViGYAN Inc. designed a wind tunnel active vibration system using balance signal feedback in low speed wind tunnel [2] and also evaluated two piezoelectric damper designs for high lift load and long slender body models in transonic tunnels [7]. Reference [8] details the damper design aspects of the NASA Common Research Model (CRM) test from a sting-damping energy viewpoint.

The active vibration control researches have achieved many convincing results. However, the above mentioned studies mainly focus on the design of actuator mechanical structures and experimental evaluation. The control algorithm or controller design process has not been specifically discussed, which is the core component of the active damping system. Although some other studies [9–11] illustrated different controllers (e.g., PD, PID, BP NN, etc.) for active vibration control purpose, these algorithms were verified only through computer simulations, not with any experiment. In [12], Shao and Chen developed a controller based on time delay compensation and it was evaluated with a wind tunnel model under exciter stimulation. Even though good results were achieved, the controller did not go through real wind tunnel tests.

In order to illustrate an entire active vibration control system in wind tunnel, this paper presents the design details of PID and BP NN controllers, which are verified with a simple beam. Then, these two controllers are evaluated with a wind tunnel model under exciter stimulation and in wind tunnel flow, respectively.

The organization of this paper is as follows. In Section 2, the active damper structure is introduced; PID and BP NN controllers are developed; the bending moment of actuators is calculated. Section 3 illustrates the evaluation tests of the controllers and the active sting damper. In Section 4, some problems about the controllers and actuators are discussed. Finally, conclusions are presented in Section 5.

2. Concepts and Preparations

2.1. Structure Design and Principles of Active Damper. The cantilever sting is illustrated in Figure 1 with a cluster of two piezoelectric devices mounted inside. Aerodynamic load on the model acts at the center of pressure with zero moments. Here the lift force of the aerodynamic load is mainly taken into consideration during the following analysis. The elastic structure of the model, balance, and sting encounters this bending moment.

Piezoelectric crystal devices are substantial capacitors. When charged electrically, the crystal expands proportionally to electrical charge. If this expansion is mechanically totally restrained, then a net force occurs on the restraint. Piezoelectric actuators have a force bandwidth of 30 KHz and hence can almost instantaneously generate force from voltage. It is this force generating capability that is used for the damper. The vertical actuators, if excited electrically, can provide pitching moment at the sting section A-A. The moment occurs around the neutral bending axis of the sting and depends on force P_f and the distance "d" between centers of the actuators. The lift force induced bending moment at the actuator cross-section can be cancelled by an equal restoring moment of magnitude "$2P_f d$." Hence, the net moment at the cluster face section of sting becomes zero.

Figure 2 shows the schematic of the active damping. The sting system responds on both aerodynamic forces and moments generated by piezoelectric devices. The balance signal is used as the feedback of the control loop which is filtered by the digital filter and functions as the input of the control algorithm run by the computer. The output signal of the control law goes through the amplifier and drives the piezoelectric cluster to create restoring moment and attenuate sting vibration.

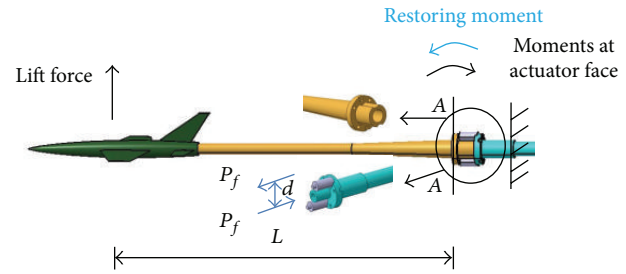

Figure 1: Sting-damping actuator design concept.

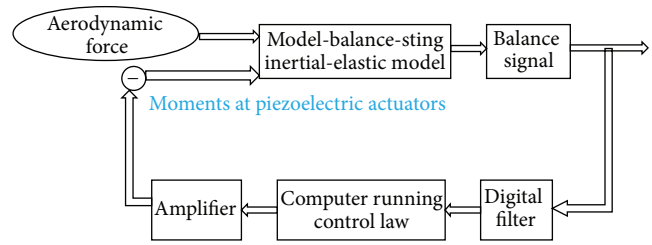

Figure 2: Schematic diagram of active sting damper control.

2.2. Control Law

2.2.1. Classical PID Controller. The PID control scheme is named after its three correcting terms whose sum constitutes the manipulated variable. Figure 3 illustrates a classical PID controller in a feedback loop. The proportional, integral, and derivative terms are summed to calculate the output of the PID controller. Defining $u(t)$ as the controller output, for the control target, $u(t)$ is also the input control signal. The final form of the PID algorithm is [13–15]

$$u(t) = K_p e(t) + K_i \int_0^t e(\tau)\, d\tau + K_d \frac{de(t)}{dt}. \tag{1}$$

The analysis for designing a digital implementation of a PID controller requires the standard form of the PID controller to be discretized. The integral term is discretized, with a sampling time Δt, and approximations for first-order derivatives are made by backward finite differences:

$$t = k \cdot \Delta t \,(k = 0, 1, 2, \ldots),$$

$$\int_0^t e(\tau)\, d\tau = \Delta t \sum_{j=0}^{k} e(j \cdot \Delta t) = \Delta t \sum_{j=0}^{k} e(j), \tag{2}$$

$$\frac{de(t)}{dt} = \frac{e(k) - e(k-1)}{\Delta t}.$$

Thus, the discrete form of PID algorithm is obtained:

$$u(t_k) = K_p e(t_k) + K_i \cdot \Delta t \sum_{j=0}^{k} e(j) + \frac{K_d}{\Delta t} [e(k) - e(k-1)]. \tag{3}$$

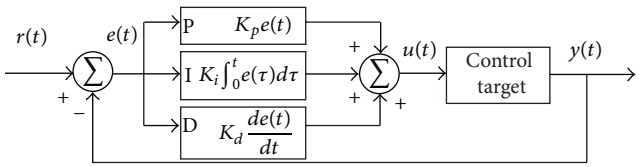

Figure 3: Block diagram of a PID controller in a feedback loop.

Classical PID controller has been widely used in engineering domain due to its simple structure. However, PID tuning, the adjustment of its control parameters (K_p, K_i, K_d) to the optimum values for the desired control response, is a difficult problem, even though there are only three parameters, and in principle is simple to describe. To design and tune a PID controller appear to be conceptually intuitive but can be hard in practice. The fundamental difficulty with PID control is that it is a feedback system, with constant parameters and no direct knowledge of the process; thus, overall performance is reactive and a compromise.

2.2.2. BP NN Controller. In this paper, a simple back propagation neural network is used to realize the function of a classical PID controller. Figure 4 shows a BP NN controller in a feedback loop. This BP NN consists of three layers. The first layer (i) is an input layer having two neurons with the process value y and desired value r as inputs correspondingly. The second layer (j) is comprised of three hidden neurons whose activation functions convert the neurons' weighted inputs to their outputs separately, which are similar to the proportional, integral, and derivative terms in classical PID controller. The third layer (h) is called output layer with one neuron whose output value is the output of the whole neural network. Weights, W_{ij} and W_{jh}, manipulate the data in the calculations, which are stored in the synapses connecting neurons of different layers.

The 3-layer BP NN's working process is illustrated schematically in Figure 5. In the beginning, the desired value r and the process value y are initialized. The initial error $e(0)$ is determined by $r(0)$ and $y(0)$, which are constants at the initial time of clock. Then, the output values of hidden and output layers are calculated, respectively [16].

Input layer:

$$\begin{aligned} x_1'(k) &= r(k), \\ x_2'(k) &= y(k), \\ y_i'(k) &= x_i'(k). \end{aligned} \tag{4}$$

Hidden layer:

$$\begin{aligned} x_j''(k) &= \sum_{i=1}^{2} W_{ij}(k)\, y_i'(k), \\ y_1''(k) &= x_1''(k), \\ y_2''(k) &= x_2''(k) + x_2''(k-1), \\ y_3''(k) &= x_3''(k) - x_3''(k-1). \end{aligned} \tag{5}$$

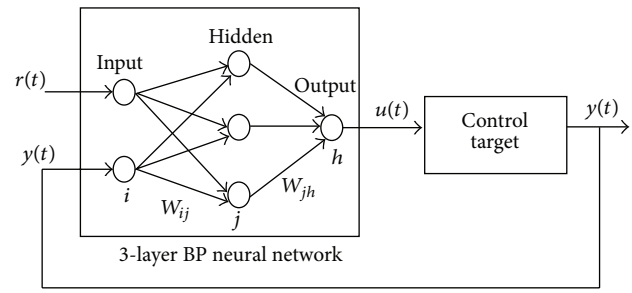

Figure 4: Schematic diagram of a BP NN controller in feedback loop.

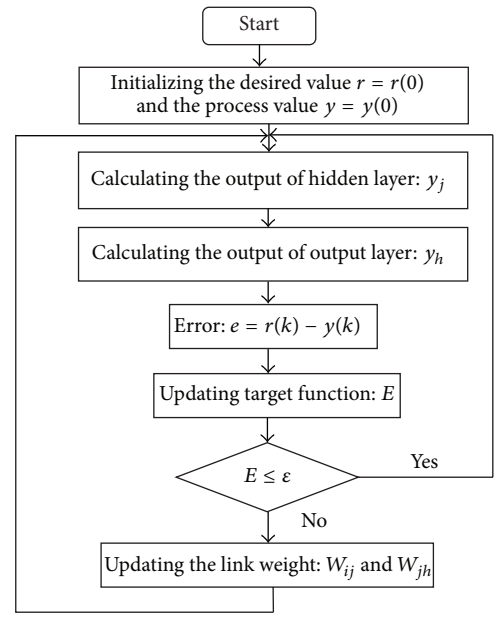

Figure 5: Flow chart of 3-layer BP NN working process.

Output layer:

$$\begin{aligned} x_h'''(k) &= \sum_{j=1}^{3} W_{jh}(k)\, y_j''(k), \\ y_h'''(k) &= x_h'''(k). \end{aligned} \tag{6}$$

Then the error e is renewed which equals the difference between the desired value r and the process value y. After that, the target function E, a function of error e (e.g., e^2), is updated and is compared with a given small number ε, 0.1, for instance, which is empirically determined by the experiment's requirement. If the value of target function is smaller than or equal to ε, then the process starts again from the beginning.

On the other hand, the link weights, W_{ij} and W_{jh}, need to be changed with iteration functions before the process starts again when E is smaller than ε. The iteration of link weights is called back propagation, through which the contribution of the P, I, and D terms to the controller output can be automatically adjusted so that output of the whole system could reach the setting value.

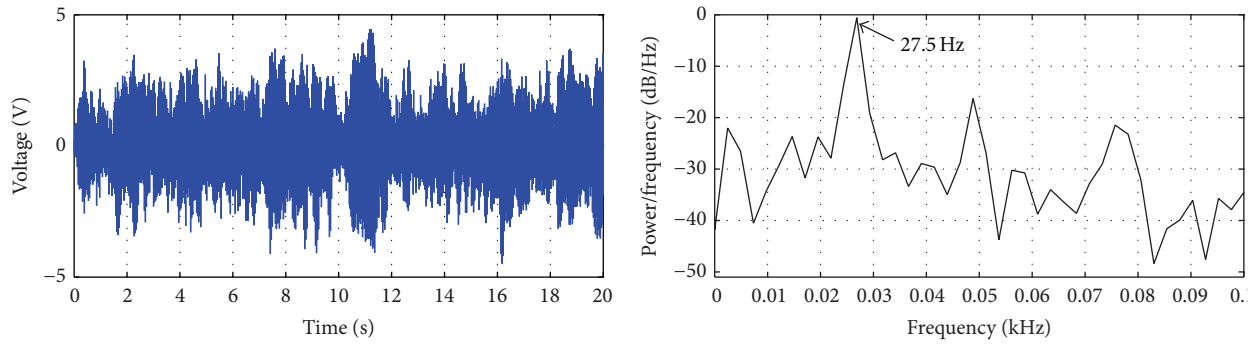

Figure 6: (a) shows time plot of balance signal without control ON and (b) shows the PSD estimation of the time plot.

Iteration functions:

$$W_{jh}(k+1) = W_{jh}(k) - \alpha \frac{\partial E}{\partial w_{jh}},$$
$$W_{ij}(k+1) = W_{ij}(k) - \beta \frac{\partial E}{\partial w_{ij}}. \quad (7)$$

In general, the BP NN is an adaptive system with back propagation, where the control parameters or link weights can be updated in real time to optimize the performance of the controller which is difficult and time consuming for classical PID algorithm. Theoretically, the drawbacks and limitations of classical PID are overcome by BP NN.

2.3. Bending Moment Calculation. The bending moment at the cross-section A-A in Figure 1 was estimated using finite element method when a sine wave force was acting on the aerodynamic center of the model.

After a series of tests in wind tunnel with active control OFF, the balance signal was recorded. Figure 6 shows one of the time plots of balance signal without active control and its PSD estimation, while the former shows the amplitude of vibration in time domain and the latter illustrates the energy contribution of different frequencies in frequency domain. The PSD estimation is given by the following formula [17]:

$$S(f) = \frac{1}{F_S N} \left| \sum_{n=1}^{N} x_n \mathbf{e}^{-j(2\pi f/F_s)n} \right|^2. \quad (8)$$

When $S(f)$ is expressed in decibel, then

$$S(f)_{\mathrm{dB}} = 10 \log_{10} S(f). \quad (9)$$

According to these time plots and power spectra, the maximum amplitude of vibration and the mainly contributing frequency were determined. Additionally, a finite element modal analysis was carried out to evaluate sting mode frequency. The sting model structure tends to vibration at around 28.1 Hz, which is close to mainly contributing frequency at 27.5 Hz. Finally, a sine wave force with 64 N peak-to-peak amplitude and 27.5 Hz frequency was used. This sine wave force was also used in the ground tests referred to Section 3.2. Figure 7 shows the sting system with a sine wave force acting on it which is the load of the finite element model.

The bending moment at section A-A was calculated by numerical integration with stress values of some critical points at the section and the stress values were extracted from a finite element transient response resulting from sine wave force. Figure 8 shows the simplified section A-A with several critical points on the left and also illustrates the transient stress response of one critical point on the right.

The driving force needed for each piezoceramic actuator to generate equivalent restoring moment was calculated from the moment when the distance between centers of actuators was given. Then, a proper type of actuator was chosen and finally used in the active sting damper.

3. Experimental Setup and Results

3.1. Control Algorithm Verification

3.1.1. Experiment Setup. The effectiveness of both classical PID and BP NN control algorithm was initially evaluated in the laboratory with an aluminum cantilever beam instead of the sting in the wind tunnel. Diagram of the experiment setup and a photograph of a cantilever beam stimulated by a fan mounted on a fixed basis in the lab are shown in Figure 9.

A 350 mm long × 40 mm wide × 2 mm thick aluminum beam was fabricated for the algorithm verification tests. The length of the beam, with comparatively low elastic modulus, is much larger than the width and thickness, which means that the beam tends to vibrate with larger amplitude in the thickness direction [18, 19].

A pair of PZT5H piezoelectric plates was fixed at the opposite surfaces of the beam near the end. The upper piezoelectric plate was used as a sensor to monitor the amplitude of beam vibration as the voltage generated by this plate was proportional to the deformation or strain of the beam at the plate's position. This deformation was linearly amplified and shown as a large displacement at the beam tip. The signal from the plate was acquired by the data acquisition card in the computer as the input of the control law. The opposite plate was used as an actuator connected to the amplifier which magnified the output of the control algorithm.

All the control laws were implemented in a National Instruments Labview platform with graphic code. The codes

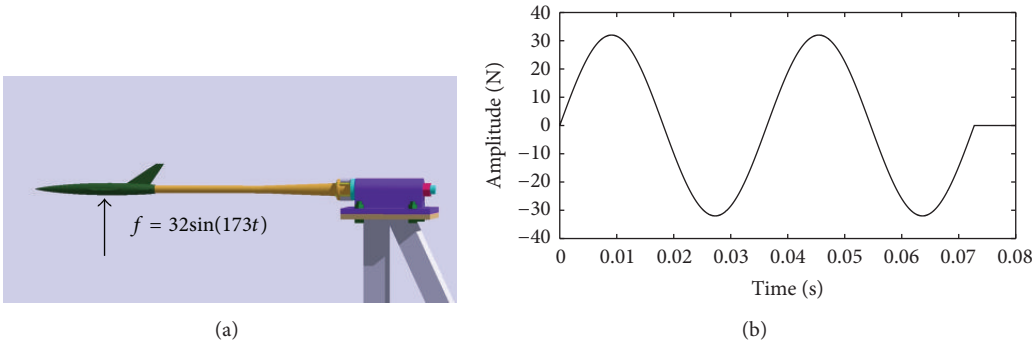

Figure 7: (a) and (b) show diagram of the sting system and a sine wave force, respectively.

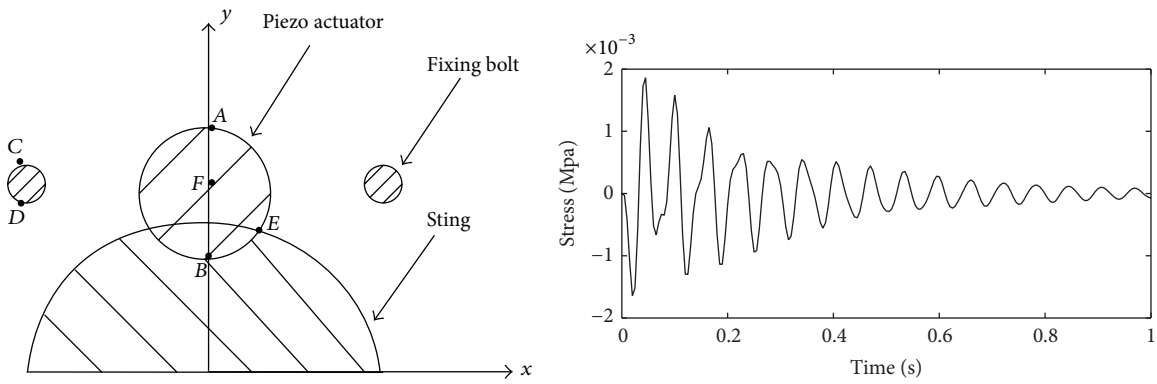

Figure 8: (a) shows diagram of cross-section at sting end and (b) shows the transient response at point A of the section.

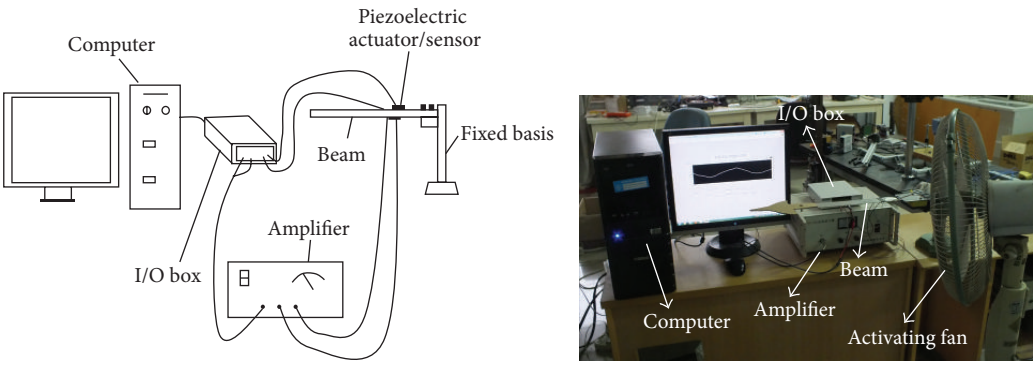

Figure 9: Diagram of the experiment setup (a), photograph of the testing system (b).

Table 1: Fan properties.

Property	Value
Rated power	50 W
Air quantity	1.03 m^3/s
Maximum wind velocity	3.07 m/s

consisted of analog-to-digital conversion and digital-to-analog conversion routines, display, keyboard control, and control laws. A cycle time of 5 kHz on all the channels was realized.

Here and in the following experiments, a National Instruments PCIe-7841R data acquisition card, with 8 analog input and output channels, was used. The detailed properties of the stimulation fan and PZT5H plates are listed in Tables 1 and 2.

3.1.2. Fan Stimulation Test Results. Tests were conducted with the active control OFF and then repeated with the active control ON. Figure 10 shows the results of the tests conducted with and without active control.

Table 2: PZT5H properties (plates).

K_{31}	K_{15}	D_{31} (10^{-12} C/N)	$S^E{}_{11}$ (10^{-12} m^2/N)	$S^E{}_{33}$ (10^{-12} m^2/N)	ρ (kg/m^3)
0.41	0.68	550	16.7	21.5	7600

The response in Figure 10 shows that the oscillations, without active damper on, have been suppressed by a PID controller. The controller has been effective in reducing the 11 Volt peak-to-peak oscillations without active control down to about 1 Volt. The STD of the data obtained before and after active control ON is 1.936 Volt and 0.196 Volt, respectively, which indicates how much variation from the average exists. That is, the oscillation amplitude, which is the displacement of the beam, is reduced by over 89%.

Figure 11 illustrates that the oscillations are successfully attenuated when the active control is on during the BP NN controller testing. Under the fan continuous stimulation, the BP NN controller brings the STD value of the data obtained with active damping down to 0.486 Volt while the original STD value is 1.936 Volt without control. There is a STD reduction of around 75% during the 10 s experiment duration. The STD value of BP NN control is nearly 0.3 Volt larger than that of classical PID control as the signals are excessive with 17 Volt peak-to-peak high frequency oscillations within the first 0.05 s which is very short compared with the whole test. When the first 0.05 s signal is cancelled from the analysis, the STD value of the rest signal would be 0.199 Volt which is similar to PID control. During this short period of time, the so-called "Back Propagation" takes effect and the link weights of the network keep changing with iteration functions until a setting value is reached. Accordingly, from 0.05 s onwards, the magnitude of the signals is always below 0.6 Volt and remains steady when the system is converged.

In summary, both of the classical PID controller and the BP NN controller perform well in the algorithm verification tests with over 75% STD value, for example, vibration amplitude reduction despite the short unstable convergence process of BP NN.

3.2. Active Damping System Evaluation. The effectiveness of the sting-damping devices was verified in a series of experiments carried out both in the laboratory and the wind tunnel facility. The experiments were part of a multiphase series of tests. Two phases of evaluation of the effectiveness of the sting-damping devices are presented.

3.2.1. Ground Tests of System. The first phase of tests was aimed at driving the sting system into resonance mechanically by using an exciter acting on the aerodynamic center of the model on the floor of the laboratory. This test involved mounting an aircraft model at zero angle of attack to the sting, which was on a rigid support fixed on a terrace groove with mounting bracket. The exciter was driven by an amplified 27.5 Hz sine wave, as mentioned in Section 2.3, from a function generator. The model sting mode is excited by the exciter creating steady state sting oscillations.

Figure 12 shows the photograph of the model-balance assembly in the laboratory with the stimulating exciter and

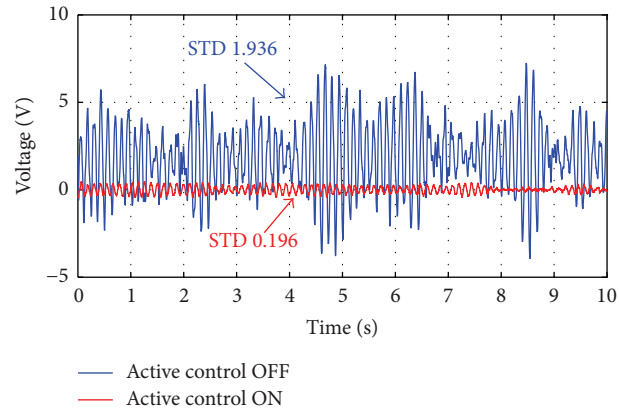

Figure 10: Cantilever beam response with PID control ON and OFF for fan stimulation.

Table 3: Exciter characteristics.

Property	Value
Maximum force	⩾50 N
Frequency range	0~3000 Hz
Maximum amplitude	$\pm 5 \times 10^{-3}$ m

Table 4: Piezoelectric actuator properties (cluster).

Property	Value
Maximum displacement	2.7×10^{-5} m
Nominal pushing force	3500 N
Resonant frequency	3.0×10^{4} Hz
Length	0.028 m

other experimental devices. A 3-component balance was used here to measure the vertical displacement of the model, as the feedback signal. Here assume that the voltage signal from the balance is proportional to the vertical displacement of the model, as it deforms similar to the cantilevered beam in Section 3.1. Then, no additional displacement sensor is needed, which is convenient in the wind tunnel experiment. Other main devices include one 8-channel lowpass filter (type: CM3508), one 3-channel amplifier (type: XE-503.00), and two piezoelectric actuators (type: PSt 150/10/20 VS15). The specific characteristics of exciter and piezoelectric cluster are detailed in Tables 3 and 4.

The exciter drive system was run initially without active damping and then active damping was imposed. Figure 13 shows the response of the balance signals to the active damper which is proportional to the normal force. The balance signals plot clearly shows the mode attenuation realized by active control with classical PID and BP NN controller. The convergence process of BP NN takes about 0.5 s before the controlled signals become steady while only 0.2 s is consumed

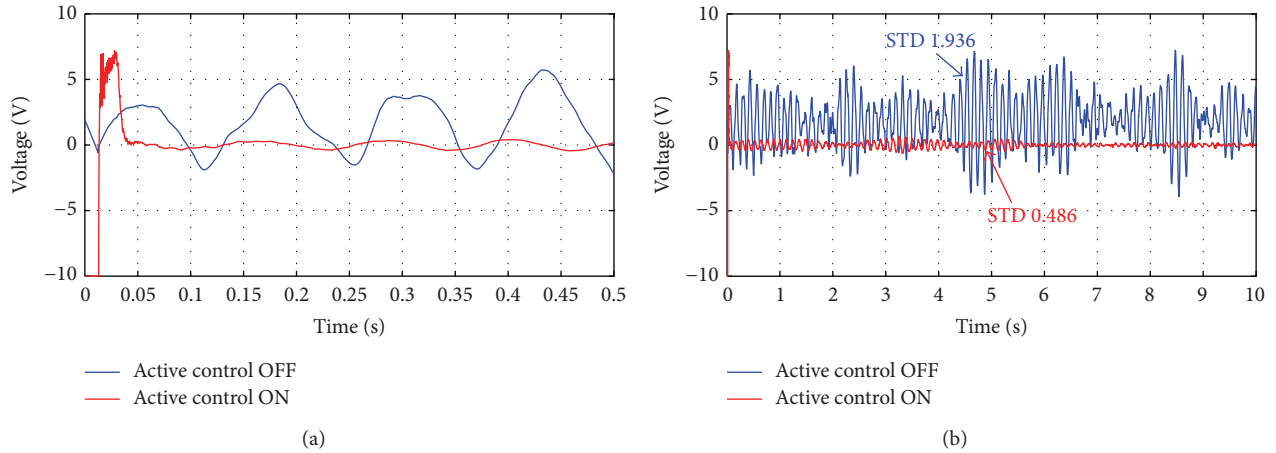

Figure 11: Cantilever system response during BP NN controller testing.

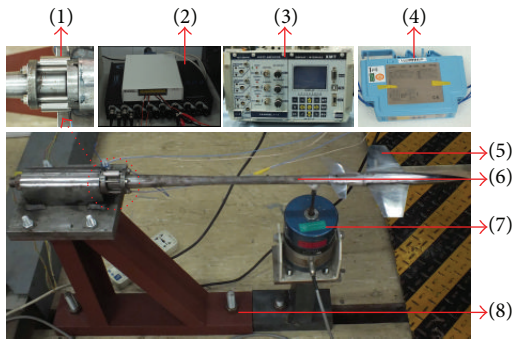

(1) Piezoelectric actuators
(2) Lowpass filter
(3) Amplifier
(4) Strain gauge input module
(5) Wind tunnel model
(6) Sting
(7) Exciter
(8) Ground support structure

Figure 12: Ground support structure and experimental devices.

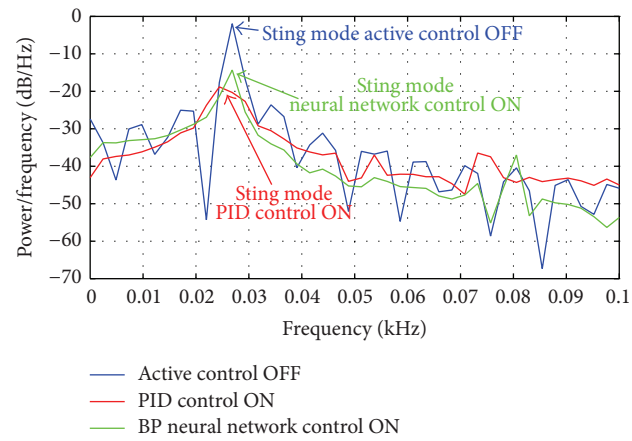

Figure 14: Attenuation of sting mode by sting damper during exciter stimulation tests.

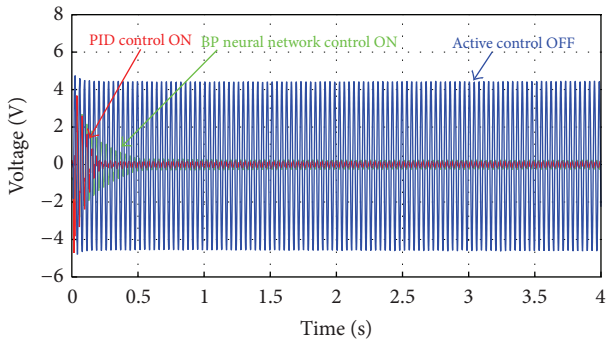

Figure 13: Time history plots from exciter stimulation tests of active sting damper with active control ON/OFF.

for PID control law to achieve the similar effect, the vibration amplitude reduced by over 95%. Figure 14 illustrates the PSD estimates of the balance signals. The spectra show that the sting mode has been successfully attenuated by about 12 dB/Hz and 18 dB/Hz for BP NN and PID controllers separately, for the frequency of analysis of 27.5 Hz. That is, according to Section 2.3, the energy contribution of 27.5 Hz is reduced by 94% for BP NN and 98% for PID.

In general, the ground testing results indicate that both the algorithms and relative hardware perform well in the real active damper.

3.2.2. Wind Tunnel Tests of System. In the second phase of testing, the sting model structure was mounted on the wind tunnel model attitude system so that the angle of attack of the model could be changed in the wind tunnel verification tests. Instead of an exciter, a metal plate was located in front of the model to create wideband disturbance in inlet flow. The photograph of the model-balance assembly in the open jet with the fixed plate upstream is shown in Figure 15. Figure 16 illustrates the experiment setup of the active damping system evaluation tests in wind tunnel while the schematic diagram of the active sting damper has already been shown in Figure 2.

Two types of experiments were conducted within the second phase of testing. In the first type of experiment, the angle of attack of the model is kept at 0 deg., when

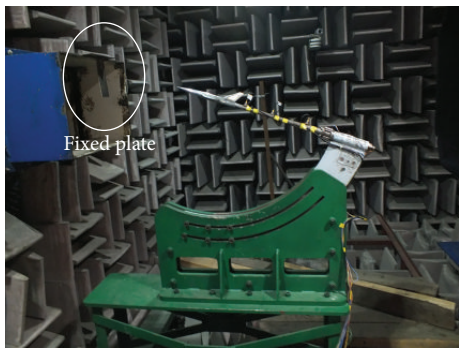

Figure 15: Photograph of model sting system installed in a low speed acoustic wind tunnel.

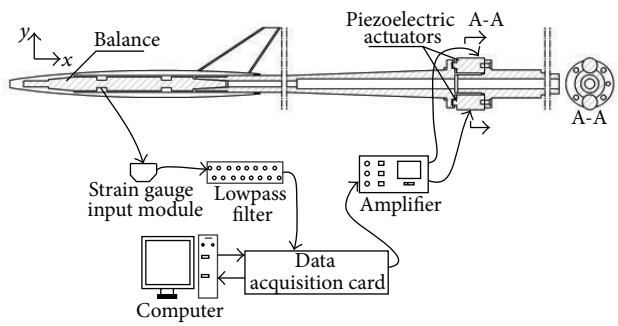

Figure 16: Diagram of the wind tunnel evaluation experiment setup.

the tunnel is run at wind velocities of 15 m/s, 20 m/s, 25 m/s, and 30 m/s. The active control damper performance, with and without the damper being switched on, is shown in plots in Figure 17. The two axes of the diagram are velocity and STD value of balance signals which indicates the magnitude of model oscillations. The plots clearly show that the model-sting vibration is alleviated by over 40% for both PID and BP NN control for almost all the different velocities.

When the wind velocity is 25 m/s, the obtained data, with and without active control, are displayed as time history plots in Figure 18. The STD value of balance signals drops to 0.63 Volt and 0.88 Volt for PID and BP NN control, respectively, when the original value is 1.46 Volt without control which also can be seen in Figure 17. The PSD estimates of the balance signals are illustrated in Figure 19 which shows that the sting mode is successfully attenuated by over 17 dB/Hz reduction for BP NN and almost 20 dB/Hz for PID. That is, the sting mode frequency energy contribution is decreased by over 98% for both two controllers. The second mode around 50 Hz is caused by the noise from power which does not exist in real structure.

The second type of experiment is carried out with a constant incoming wind velocity of 25 m/s when the angle of attack varies from 0 deg. to 20 deg. with a step increase of magnitude 5 deg. Figure 20 shows plots of the STD values of balance signals with and without active control at 5 different angles. The results are similar to that in Figure 17. Both PID and BP NN perform well in attenuating the sting oscillations by reduction of over 40% in most cases.

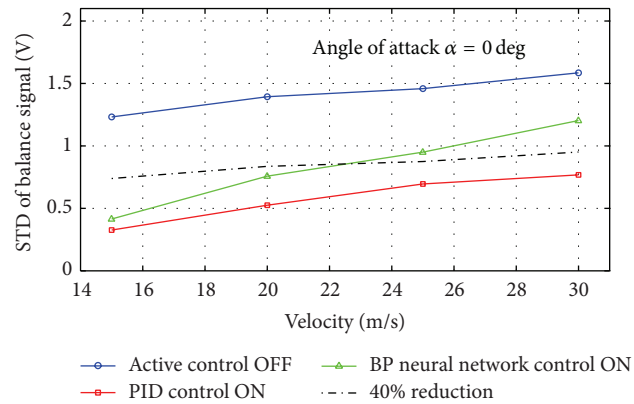

Figure 17: Pitch performance of active damper with model at $\alpha = 0$, balance signal STD versus velocity with active control ON/OFF.

In general, the amplitude of sting vibration is reduced successfully over a wide range of wind velocities and angles of attack for both PID and BP NN control in wind tunnel evaluation tests.

4. Discussions

Under single frequency sine wave excitation, similar control effect was achieved by PID and BP NN controller. While the PID control has shorter settling time, the adjustment of its control parameters to the optimums can be hard in practice and time consuming, which may take hours or even days. This drawback is overcome by BP NN control, which is a self-tuning controller. The optimum control parameters are achieved automatically through back propagation process, which takes less than one second in ground tests. So when the well-tuned control parameters are already available, the PID control should be preferred; otherwise, BP NN control should be chosen.

At wind tunnel tests for PID control, at each new condition, new velocity, or new angle of attack, the control parameters need to be adjusted manually, which takes a lot of time. But for BP NN control, it is unnecessary and that is what makes BP NN more advantageous over PID. Additionally, the self-tuning or continuous back propagation process makes BP NN more sensitive to the disturbance in the airflow leading to unstable response of the system. In this paper, one simple 3-layer BP NN with 3 hidden neurons was used as controller. More hidden neurons and layers could be added to improve the robustness of BP algorithm. The relationship between robustness of the controller and the BP NN structure in the wind tunnel active vibration control could be a good future research direction.

In this work, for verification and simplicity, the final evaluation tests were carried out in a low speed acoustic wind tunnel, where the pitch sting Eigenmode is the main vibration source. Thus, only one pair of actuators, arranged in pitch direction, was used and verified to attenuate the oscillation successfully. However, the following situation should also be paid attention to. In high speed wind tunnels, transonic and supersonic, for example, high-level vibration always

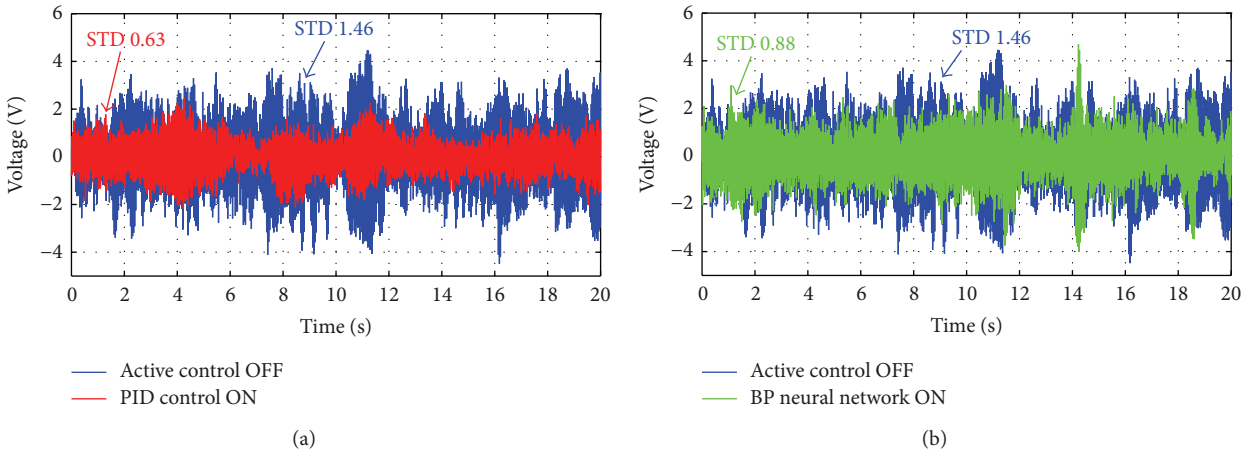

FIGURE 18: Time plots of balance signals with active control ON/OFF at $v = 25$ m/s, (a) for PID control and (b) for BP NN control.

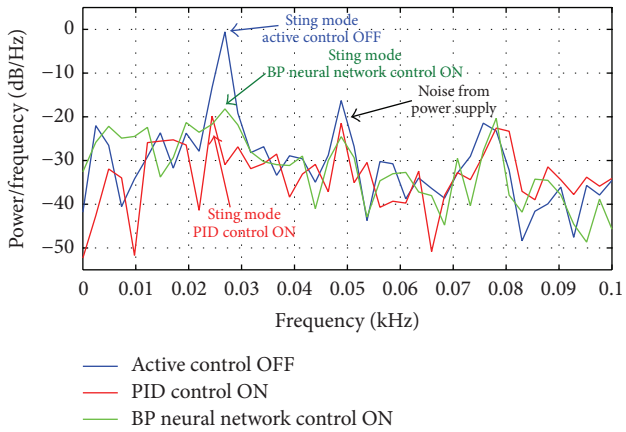

FIGURE 19: Model response to unstable airflow with active control ON/OFF in wind tunnel evaluation tests.

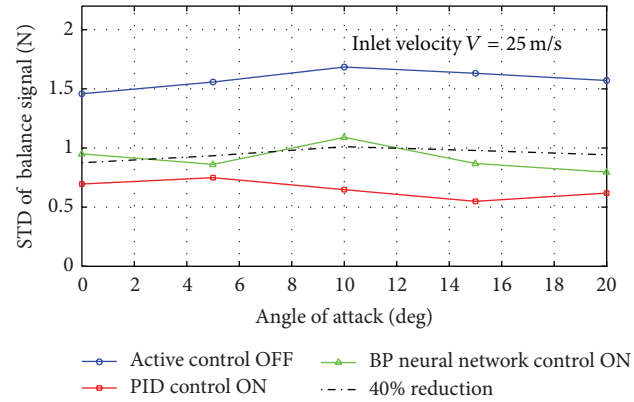

FIGURE 20: Plots of active damper pitch performance throughout an angle of attack sweep, balance signal STD versus angle of attack with active control ON/OFF.

exists, which can be due to excitation that contains a fair degree of randomness and wide dynamic frequency range. In that case, more than one of the six dominate Eigenmodes would most likely be activated. Thus, 2, 3, or even more pairs of actuators, as shown in Figure 21, would be required to eliminate the extra Eigenmodes. Taking configuration 2 as an example, the additional pair of actuator in yaw direction could attenuate the yaw and coupled roll mode of the sting. On the other hand, it should not be forgotten that more actuators mean more output channels and increasing complicity of the algorithm. Compromise should be made based on the balance of test requirements and costs of both software and hardware in the future research.

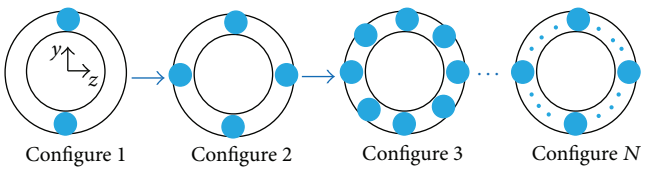

FIGURE 21: Configurations of piezoelectric actuators.

5. Conclusions

In this paper, the methodology of designing a sting damper capable of attenuating the sting mode due to low damping is developed, by using a pair of piezoelectric actuators embedded at the end of the sting. The presented approach uses the balance signal as feedback. Therefore, in the active damping system, no additional sensors, accelerometer, or speedometer, are required, which is convenient in wind tunnel test. A classical PID and a 3-layer BP NN controller have been designed in detail. The feasibility and effectiveness of the control algorithms have been verified with a simple cantilever beam system and the actuators have been chosen according to the bending moment estimation. In active damping evaluation tests, it is shown that, for both two controllers, up to 95% of displacement response of the sting mode can be eliminated under exciter stimulation and 98% of the sting mode frequency energy can be cancelled in wind tunnel tests.

In conclusion, the commercially available high force piezoelectric devices have made the design and fabrication of active sting dampers possible to reduce sting oscillations significantly. Such damper has demonstrated an ability to solve the sting vibration problems encountered in wind tunnel testing with proper control algorithm.

Nomenclature

PID:	Proportional-integral-derivative controller
BP NN:	Back propagation neural network controller
STD:	Standard deviation
K_p, K_i, K_d:	Proportional, integral, derivative gain
e:	Error: Desired value (r), process value (y)
t:	Time
τ:	Variable of integration
Δt:	Sampling time
W_{ij}, W_{jh}:	Link weights of neural network
x_i', x_j'', x_h''':	Input values of input, hidden, and output layers ($i = 1, 2$; $j = 1, 2, 3$; $h = 1$)
y_i', y_j'', y_h''':	Output values of input, hidden, and output layers ($i = 1, 2$; $j = 1, 2, 3$; $h = 1$)
α, β:	Neural network learning velocity constant
PSD:	Power spectral density
S:	Periodogram, an estimate of the PSD
f:	Frequency variable in Hz
F_s:	Sampling frequency
$x_1, x_2, \ldots, x_N$:	Signal sequence
K_{31}, K_{15}:	Electromechanical coupling coefficient
D_{31}:	Piezoelectric constant
S_{11}^E, S_{33}^E:	Elastic compliance constant
ρ:	Density.

Conflict of Interests

The authors declare that there is no conflict of interests regarding the publication of this paper.

Acknowledgments

This study was supported by the NUAA Fundamental Research Funds (no. NS2013010), National Science Foundation of China (no. 50911140286), Foundation of Graduate Innovation Center in NUAA (no. kfjj130105), and the Fundamental Research Funds for the Central Universities.

References

[1] C. P. Young, T. G. Popernack, and B. B. Gloss, "National transonic facility model and model support vibration problems," in *Proceedings of the AIAA 16th Aerodynamic Ground Testing Conference*, Seattle, Wash, USA, June 1990.

[2] S. Balakrishna, H. Houlden, D. H. Butler, and R. White, "Development of a wind tunnel active vibration reduction system," in *Proceedings of the 45th AIAA Aerospace Sciences Meeting and Exhibit*, Reno, Nev, USA, January 2007.

[3] C. P. Young Jr., D. W. Hergert, T. W. Butler, and F. M. Herring, "Buffet testing in National Transonic Facility," in *Proceedings of the AIAA 17th Aerospace Ground Testing Conference*, Nashville, Tenn, USA, July 1992.

[4] W. B. Igoe and F. T. Capone, "Reduction of wind tunnel model vibration by means of a tuned damped vibration absorber installed in a model," NASA Technical Memorandum: NASA TMX-1606.

[5] P. H. Fuykschot, "The use of friction springs for damping model vibrations," in *NLR STA Proceedings*, National Aerospace Laboratory, April 1999.

[6] H. Fehern, U. Gnauert, R. Wimmel, G. Hefer, and D. Schimanski, "Validation testing with the active damping system in the European transonic windtunnel," in *Proceedings of the 39th AIAA Aerospace Sciences Meeting and Exhibit*, Reno, Nev, USA, January 2001.

[7] S. Balakrishna, D. H. Butler, R. White, and W. A. Kilgore, "Active damping of sting vibrations in transonic wind tunnel testing," in *Proceedings of the 46th AIAA Aerospace Sciences Meeting and Exhibit*, Reno, Nev, USA, January 2008.

[8] S. Balakrishna, D. H. Butler, M. J. Acheson, and E. R. White, "Design and performance of an active sting damper for the NASA common research model," in *Proceedings of the 49th AIAA Aerospace Sciences Meeting Including the New Horizons Forum and Aerospace Exposition*, Orlando, Fla, USA, January 2011.

[9] F. J. Darsivan, W. Martono, and W. F. Faris, "Active engine mounting control algorithm using neural network," *Shock and Vibration*, vol. 16, no. 4, pp. 417–437, 2009.

[10] Y.-L. Zhou, Q.-Z. Zhang, T. Zhang, X.-D. Li, and W.-S. Gan, "Active noise control using a functional link artificial neural network with the simultaneous perturbation learning rule," *Shock and Vibration*, vol. 16, no. 3, pp. 325–334, 2009.

[11] Q. Zhang and Y. Jia, "Active noise feedback control using a neural network," *Shock and Vibration*, vol. 8, no. 1, pp. 15–19, 2001.

[12] M. Q. Shao and W. D. Chen, "Active vibration control in a cantilever-like structure: a time delay compensation approach," *Journal of Vibration and Control*, vol. 19, no. 5, pp. 674–685, 2012.

[13] K. J. Åström and T. Hägglund, *PID Controllers: Theory, Design, and Tuning*, Instrument Society of America, Raleigh, NC, USA, 2nd edition, 1995.

[14] G. F. Franklin, J. D. Powel, and A. Emami-Naeni, *Feedback Control of Dynamic Systems*, Prentice Hall, Upper Saddle River, NJ, USA, 4th edition, 2003.

[15] R. C. Hibbeler, *Engineering Mechanics-Dynamics*, Prentice Hall, Singapore, 3rd edition, 2004.

[16] D. E. Rumelhart and J. L. McClelland, *Parallel Distributed Processing*, vol. 1-2, The MIT Press, Cambridge, Mass, USA, 1986.

[17] P. Stoica and R. L. Moses, *Introduction to Spectral Analysis*, Pearson Education, Upper Saddle River, NJ, USA, 1997.

[18] G. L. C. M. Abreu, J. F. Ribeiro, and V. Steffen Jr., "Experiments on optimal vibration control of a flexible beam containing piezoelectric sensors and actuators," *Shock and Vibration*, vol. 10, no. 5-6, pp. 283–300, 2003.

[19] A. Nandi, S. Neogy, S. Bhaduri, and H. Irretier, "Vibration attenuation by a combination of a piezoelectric stack and a permanent magnet," *Shock and Vibration*, vol. 19, no. 4, pp. 719–734, 2012.